

Revisiting the Amati and Yonetoku Correlations with *Swift* GRBs

H. Zitouni • N. Guessoum • W. J. Azzam

Abstract

We use a sample of *Swift* gamma-ray bursts (GRBs) to analyze the Amati and Yonetoku correlations. The first relation is between $E_{p,i}$, the intrinsic peak energy of the prompt GRB emission, and E_{iso} , the equivalent isotropic energy. The second relation is between $E_{p,i}$ and L_{iso} , the isotropic peak luminosity. We select a sample of 71 *Swift* GRBs that have a measured redshift and whose observed E_p^{obs} is within the interval of energy 15-150 keV with a relative uncertainty of less than 70%. We seek to find correlation relations for long-duration GRBs (LGRBs) with a peak photon flux $P_{ph} \geq 2.6$ ph/cm²/s. Uncertainties (error bars) on the values of the calculated energy flux P , the energy E_{iso} , and the peak isotropic luminosity L_{iso} are estimated using a Monte Carlo approach. We find 27 *Swift* LGRBs that satisfy all our constraints. Results of our analyses of the sample of 71 GRBs and the selected subsample (27 GRBs) are in good agreement with published results. The plots of the two relations for all bursts show a large dispersion around the best straight lines in the sample of 71 LGRBs but not so much in the subsample of 27 GRBs.

Keywords gamma-rays: bursts; methods:statistical

H. Zitouni

Faculté des sciences, Université Dr Yahia Fares, Pôle urbain, Médéa, Algeria.

N. Guessoum

Department of Physics, College of Arts & Sciences, American University of Sharjah, UAE.

W. J. Azzam

Department of Physics, College of Science, University of Bahrain, Bahrain.

1 Introduction

Gamma-ray bursts (GRBs) are sudden, and very brief, outbursts of high-energy gamma photons that appear randomly in time and space. They were serendipitously discovered in 1967, and are of great importance because they are currently the most luminous and distant sources in the universe. They hold great promise as cosmological probes of the early universe, since their flux is unencumbered by extinction due to dust (Ghirlanda et al. 2006; Azzam and Alothman 2006a,b; Capozziello and Izzo 2008; Demianski and Piedipalumbo 2011). One of the most important elements in the detection of GRBs is the redshift, z , since its determination is necessary in order to investigate all the intrinsic characteristics of GRBs. It is generally determined by the identification of absorption lines in the optical afterglow spectra, when they are bright enough. Large terrestrial telescopes equipped with spectrographs working in the infrared or the optical domains are the best places to perform this task.

Over the past decade, several GRB energy and luminosity relations have been discovered, in which an observed parameter correlates with an intrinsic parameter. Some of these relations are obtained from the light curves, like the lag-luminosity relation (Norris et al. 2000) and the variability relation (Fenimore and Ramirez-Ruiz 2000), while others are extracted from the spectra and include the Amati relation (Amati et al. 2002; Amati 2006; Amati et al. 2008, 2009), the Ghirlanda relation (Ghirlanda et al. 2004), the Yonetoku relation (Yonetoku et al. 2004; Ghirlanda et al. 2010), and the Liang-Zhang relation (Liang and Zhang 2005).

In this work, we use a sample of *Swift* GRBs that we selected according to a specific criterion (described in Section 2) in order to investigate two of these correlations: the Amati relation, which is a correlation between the intrinsic (i.e., rest-frame) peak energy, $E_{p,i}$,

in a burst's νF_ν spectrum and its equivalent isotropic energy, E_{iso} ; and the Yonetoku relation which is a correlation between $E_{p,i}$ and a burst's isotropic peak luminosity, L_{iso} .

A detailed description of our sample selection is provided in Section 2, which is followed by a presentation of our spectral analysis and results in Sections 3 and 4, respectively. A discussion of our results including a comparison with what has been done by others is given in Section 5, and our conclusions are provided in Section 6.

2 Sample Selection

We use the *Swift* GRBs data that is published on the official websites^{1,2}. The first one presents the observational results characterizing the overall GRB: peak flux, fluence, duration, redshift, host galaxy, as well as data on afterglows. The second website provides more details on the energy spectrum and the time profile in different energy bands, for different time resolutions. The data are all provided with their uncertainties (error bars). We simply use that data to check for the validity of the Amati and Yonetoku correlations. Bursts that interest us are therefore long-duration GRBs (LGRBs) with measured redshifts.

As of 25/09/2013, *Swift* observed 809 GRBs, of which 703 are long-duration GRBs. Among these 703 LGRBs, only 236 have measured redshifts, of which 17 are “approximate” redshifts (060708, 071020, 050904, 110726A, 100704A, 090814A, 070721B, 060912A, 070306, 050803, 120521C, 060116, 100728B, 081222, 060502A, 080430, and 050802), which leaves 219 LGRBs with well determined redshifts. We note that in cases where several methods for the determination of a redshift were possible, we have adopted the values given by the absorption method, which is generally the most precise (with four significant figures).

In Figure 1 we plot the distribution of 219 LGRBs detected by *Swift* up to 25/09/2013. Of these, we select the bursts that have an energy E_p^{obs} in the *Swift* range [15-150] keV, with a relative accuracy of at least 70%. This selection filter leaves us with 71 GRBs. Among these, 57 have both L_{iso} and $E_{p,i}$ values and thus can be used for testing the Amati relation, while 56 have E_{iso} and $E_{p,i}$ values and thus can be used for testing the Yonetoku relation. 42 GRBs are common to both relations. The last constraint that we apply in selecting *Swift* bursts is the photon flux which must be more

than the threshold $P_{ph} = 2.6$ ph/cm²/s. The sample we obtain is one of 27 “good” GRBs for our analysis. We note that these 27 bursts have been very strictly selected. The percentage of bursts that obey the observational constraints is of the order of 4% of the total number of LGRBs, and it is 13% of LGRBs with well-determined redshift.

3 Spectral Analysis

The 1-sec photon flux at the peak can be found in the *Swift* data. This flux gives the total number of photons per unit area and per unit time, regardless of their individual energies. The *Swift* energy spectrum is divided into four bands: 15-25 keV, 25-50 keV, 50-100 keV, 100-350 keV. The spectrum (photons per unit area, time, and energy) can be fitted by one of three well known functions: the Band function (Band et al. 1992), the cut-off power law (CPL), and the power law (PL). The first two are known to give very similar chi-square (χ^2) values when fitting the spectra. In the aforementioned *Swift* data web sites, only the PL and the CPL functions are given for each burst; thus, in this work, we have chosen to use the cut-off power law, which is characterized by two spectral parameters: the observed peak energy, E_p^{obs} , and the spectral index alpha (α).

$$N(E) = N_0 \left(\frac{E}{E_n} \right)^\alpha e^{-E/E_0}, \quad (1)$$

where $E_n = 50$ keV, a mid-range value in the interval 15-150 keV which is only used for normalization purposes and $E_0 = E_p^{obs}/(2 + \alpha)$. The spectral parameters E_p^{obs} and α in the CPL function are not necessarily the same as those of the Band law for a given burst. This observation has a direct effect on the two correlation relations since both of them depend on $E_{p,i}$.

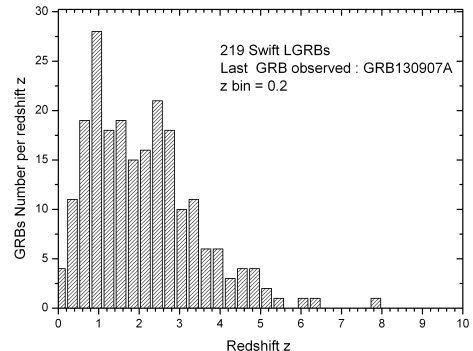


Fig. 1 GRB's distribution with redshift z , with a bin of 0.2

¹http://swift.gsfc.nasa.gov/archive/grb_table/

²http://gcn.gsfc.nasa.gov/swift_gnd_ana.html

To calculate the peak energy flux, expressed in erg/cm²/s, we use the spectral parameters that characterize the peak photons. This is given under the heading “1-s peak spectral analysis” of the *Swift* data page. We only take what relates to the CPL spectrum. Using the CPL law, the observed peak fluxes P_{ph} that are given in Table (4), are calculated theoretically using the following expression:

$$P_{ph} = N_0 \int_{E_{min}}^{E_{max}} \left(\frac{E}{E_n}\right)^\alpha e^{-E(2+\alpha)/E_p^{obs}} dE, \quad (2)$$

where $E_{min} = 15$ keV, $E_{max} = 150$ keV. P_{ph} , α and E_p^{obs} being given in Table (4). In Eq.2, the only unknown is the normalization constant N_0 , which we determine by numerically integrating the previous function, i.e.

$$N_0 = \frac{P_{ph}}{\int_{E_{min}}^{E_{max}} \left(\frac{E}{E_n}\right)^\alpha e^{-\frac{E(2+\alpha)}{E_p^{obs}}} dE}. \quad (3)$$

The peak energy flux, denoted by F_γ and calculated in erg/cm²/s, is calculated numerically through the following equations:

$$F_\gamma = \int_{E_{min}}^{E_{max}} EN(E)dE, \quad (4)$$

$$= N_0 \int_{E_{min}}^{E_{max}} E \left(\frac{E}{E_n}\right)^\alpha e^{-\frac{E(2+\alpha)}{E_p^{obs}}} dE, \quad (5)$$

$$= N_0 K E_n \int_{E_{min}}^{E_{max}} \left(\frac{E}{E_n}\right)^{\alpha+1} e^{-\frac{E(2+\alpha)}{E_p^{obs}}} dE. \quad (6)$$

A factor $K = 1.6 \cdot 10^{-9}$ is introduced to make the keV-erg conversion and $E_n = 50$ keV.

The bolometric luminosity of the 1-second isotropic peak, denoted L_{iso} , is the maximum energy radiated per unit time in all space. It is calculated by integrating the EN_E function in the energy band corresponding to the observed gamma radiation band in the source’s frame, i.e. $E_1/(1+z)$ to $E_2/(1+z)$.

Thus, the k-corrected L_{iso} is calculated via:

$$L_{iso} = 4 \pi d_L^2 \int_{E_1/(1+z)}^{E_2/(1+z)} EN(E)dE, \quad (7)$$

$$= 4 \pi d_L^2 F_\gamma k_c. \quad (8)$$

Here L_{iso} is k-corrected with the method developed by (Bloom et al. 2001). Indeed, in Eq.(7) we replace $N(E)$

by Eq.(1) and using Eq.(5) to express N_0 , we obtain:

$$\begin{aligned} k_c &= \frac{\int_{E_1/(1+z)}^{E_2/(1+z)} \left(\frac{E}{E_n}\right)^{\alpha+1} e^{-\frac{E(2+\alpha)}{E_p^{obs}}} dE}{\int_{E_{min}}^{E_{max}} \left(\frac{E}{E_n}\right)^{\alpha+1} e^{-\frac{E(2+\alpha)}{E_p^{obs}}} dE}, \\ &= \frac{\int_{E_1/(1+z)}^{E_2/(1+z)} EN(E)dE}{\int_{E_{min}}^{E_{max}} EN(E)dE}, \end{aligned} \quad (9)$$

where k_c being the proper k-correction factor (Yonetoku et al. 2004; Rossi et al. 2008; Elliott et al. 2012).

These integrals are performed numerically using the time-resolved spectral parameters given by *Swift*. The cosmological distance d_L is expressed by the following equation:

$$d_L = \frac{(1+z)c}{H_0} \int_0^z \frac{dz'}{\sqrt{\Omega_M(1+z')^3 + \Omega_L}}. \quad (10)$$

We adopt the following cosmological parameters:

$\Omega_M = 0.27$, $\Omega_L = 0.73$, and $H_0 = 70$ km/s/Mpc (Kotomatsu et al. 2009).

The total isotropic energy, denoted E_{iso} , which is emitted by a gamma-ray burst in all space, is calculated using the fluences (erg/cm²) given by the detectors in the *Swift* energy band [15- 150] keV. To calculate this, we use a cut-off power law spectrum with time-averaged spectral parameters (α_m, E_{pm}) obtained from the *Swift* data. Using the CPL function, the fluence S_{obs} , given in the fourth column in table (4), can be theoretically calculated using the following equation:

$$\begin{aligned} S_{obs} &= \int_{E_{min}}^{E_{max}} E N_i(E) dE, \\ &= N'_0 E_n T_{90}^{obs} \int_{E_{min}}^{E_{max}} \left(\frac{E}{E_n}\right)^{\alpha_m+1} e^{-\frac{E(2+\alpha_m)}{E_{pm}^{obs}}} dE, \\ &= N'_0 \int_{E_{min}}^{E_{max}} \left(\frac{E}{E_n}\right)^{\alpha_m+1} e^{-\frac{E(2+\alpha_m)}{E_{pm}^{obs}}} dE, \end{aligned} \quad (11)$$

with $E_{min} = 15$ keV, $E_{max} = 150$ keV and $E_n = 50$ keV. α_m and E_{pm}^{obs} are given in Table (4), for the time-averaged spectrum. $N_i(E)$ is the time-integrated spectrum calculated via the product of the time-averaged spectrum by T_{90}^{obs} , the observed duration of the GRB:

$$\begin{aligned} N_i(E) &= T_{90}^{obs} \times \left\{ \frac{1}{T_{90}^{obs}} \int_0^{T_{90}^{obs}} N(E, t) dt \right\}, \\ &= T_{90}^{obs} \left\{ N'_0 \left(\frac{E}{E_n}\right)^{\alpha_m} e^{-\frac{E(2+\alpha_m)}{E_{pm}^{obs}}} \right\}. \end{aligned} \quad (12)$$

In equation 11 the only unknown is the normalization constant N' ; it is determined by numerical integration,

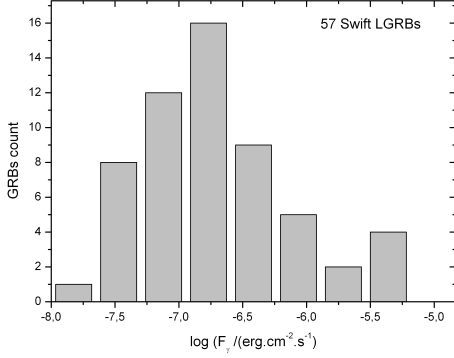


Fig. 2 Histogram of LGRBs in terms of the peak energy flux F_γ . We split the interval from $\log(F_\gamma) = 8$ to $\log(F_\gamma) = 5$ into 8 bins. 57 Swift LGRBs were used in this histogram. Here, we did not consider the constraint on the threshold on the flux: $P_{ph} \geq 2.6 \text{ ph/cm}^2/\text{s}$

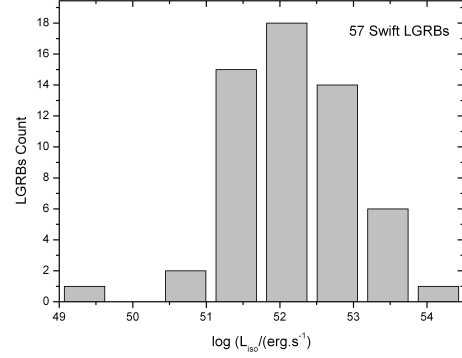


Fig. 3 Histogram of LGRBs in terms of the peak isotropic luminosity. We split the interval from $\log(L_{iso}) = 49$ to 55 into 8 bins. 57 Swift LGRBs were used. Here, we did not consider the constraint: $P_{ph} \geq 2.6 \text{ ph/cm}^2/\text{s}$

i.e.:

$$N' = \frac{S_{obs}}{\int_{E_{min}}^{E_{max}} \left(\frac{E}{E_n}\right)^{\alpha_m+1} e^{-\frac{E(2+\alpha_m)}{E_{pm}^{obs}}} dE}. \quad (13)$$

Thus, N' is used to deduce k-corrected E_{iso} :

$$\begin{aligned} E_{iso} &= \frac{4\pi d_L^2}{1+z} \int_{E_1/(1+z)}^{E_2/(1+z)} E N_i(E) dE, \\ &= \frac{4\pi d_L^2}{1+z} S_{obs} k'_c. \end{aligned} \quad (14)$$

The $(1+z)$ factor is a cosmological correction that is needed because one must use T_{90}^s (the GRB's duration in the source's frame) instead of T_{90}^{obs} : $T_{90}^s = T_{90}^{obs}/(1+z)$; [$E_1 = 1 \text{ keV}$; $E_2 = 10^4 \text{ keV}$] is the energy band in the source's frame. k'_c is the k-correction factor calculated with the parameters of the time-averaged spectrum:

$$\begin{aligned} k'_c &= \frac{\int_{E_1/(1+z)}^{E_2/(1+z)} \left(\frac{E}{E_n}\right)^{\alpha_m+1} e^{-\frac{E(2+\alpha_m)}{E_{pm}^{obs}}} dE}{\int_{E_{min}}^{E_{max}} \left(\frac{E}{E_n}\right)^{\alpha_m+1} e^{-\frac{E(2+\alpha_m)}{E_{pm}^{obs}}} dE}, \\ &= \frac{\int_{E_1/(1+z)}^{E_2/(1+z)} E N_i(E) dE}{\int_{E_{min}}^{E_{max}} E N_i(E) dE}. \end{aligned} \quad (15)$$

4 Results

4.1 Distribution of F_γ , E_{iso} and L_{iso}

In the previous sections we numerically evaluated the energy flux denoted by F_γ ($\text{erg/cm}^2/\text{s}$), the peak

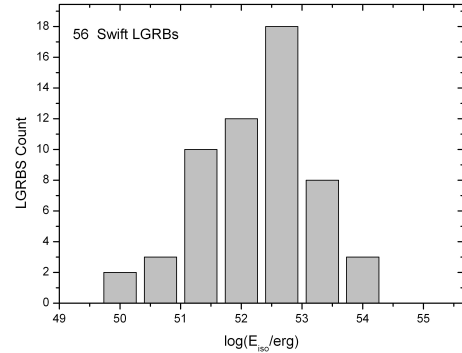


Fig. 4 Histogram of LGRBs in terms of the isotropic energy. We split the interval from $\log E_{iso} = 49$ to 55 into 7 bins. 56 Swift LGRBs were used. Here, we did not consider the constraint: $P_{ph} \geq 2.6 \text{ ph/cm}^2/\text{s}$

isotropic bolometric luminosity, L_{iso} , and the isotropic energy E_{iso} . Uncertainties over these quantities are estimated using the Monte Carlo method. We have plotted the distributions P , E_{iso} , L_{iso} in Figures 2, 3, and 4 respectively. We also obtained the distributions of the two physical quantities E_{iso} and L_{iso} in the sources' reference frames. In Figure 4, we note that E_{iso} , which represents the total energy released by the burst during its entire activity, follows a lognormal distribution, previously known (Preece et al. 2000), with a mean equal to $1.7 \times 10^{52} \text{ erg}$. Most gamma-ray bursts that are detected by other satellites are characterized by this average value.

This luminosity is different from the time-resolved peak luminosity that was calculated above.

In Figure(5) we present the correlation between L_{iso} and E_{iso} : a burst that releases a large amount of energy

is characterized by high luminosity. We note that these two quantities are correlated with a wide dispersion of the observational data.

4.2 Correlation Relations

One of the most debated issues regarding gamma-ray bursts (GRB) is the existence of a correlation relation between the spectral parameters of the prompt emission and either the total energy or the luminosity. Three robust correlations have been identified but not yet confirmed. Each involves the peak energy E_p of the spectrum νf_ν , estimated in the source's frame. This quantity is strongly correlated with: (a) the total isotropic energy E_{iso} (Amati et al. 2002; Amati 2006), (b) the isotropic luminosity L_{iso} (Yonetoku et al. 2004), and (c) the total energy collimated with the opening angle θ which is denoted by E_θ (Ghirlanda et al. 2004). The opening angle is inferred from the observed break in the temporal profile of the afterglows. In the BATSE observations, θ did not exceed ten degrees, while *Swift* observations of afterglows do not show, in most cases, such a break. Such correlations apply only in long GRBs. The spectral energy correlations have important implications for both the theoretical understanding of GRBs and for cosmological applications (Ghirlanda et al. 2004, 2005).

4.2.1 The $E_{iso} - E_{p,i}$ Relation

The relation between the energies $E_{p,i}$ and E_{iso} , discovered by Amati et al. (2002) has been the subject of several publications, even though it has not yet been fully confirmed. This topic has had several controversies. In 2002, Amati et al. (2002) came up with this relationship from a sample of 12 *Beppo-SAX* GRBs with well-determined redshifts. These researchers showed that there is a purely empirical relation between $E_{p,i}$, the peak energy of the photon spectrum νf_ν of the prompt emission, as measured in the source's frame and the total equivalent isotropic energy E_{iso} that is emitted in the energy band [1-10⁴ keV], that is the energy radiated by the source in this energy range, assuming an isotropic emission. This relation requires a redshift measurement. The redshift is necessary to know the intrinsic properties of the source, as the intrinsic peak energy is given by the relation:

$$E_{p,i} = E_p^{obs} \times (1 + z), \quad (16)$$

where E_p^{obs} is the peak energy observed by the *Swift/BAT* detectors. The Amati relation is given by:

$$\frac{E_{p,i}}{keV} = K \times \left(\frac{E_{iso}}{10^{52} \text{ erg}} \right)^m, \quad (17)$$

where K and m are constants.

For the original Amati relation, $K \approx 95$ and $m \approx 0.5$. This relation can be used to constrain cosmological parameters as well as different models aiming to explain the prompt emission. It can also provide information on the nature of the various subclasses of gamma-ray bursts (e.g., LGRB, SGRB, etc.)

We plot our results for the Amati relation in Figure (6). These plots are for 27 bursts detected by *Swift/BAT* with well determined redshifts. We plot $\log E_p$ as a function of $\log E_{iso}$. We represented two extreme lines, in fitting the 27-point distribution. From these two lines we have deduced the mean values for the line's slope and intercept. In Table (1) we give the constants K and m of Eq.17, as obtained from the following expressions:

$$K = 10^{(52a+b)}, \quad (18)$$

$$m = a. \quad (19)$$

We also give the original results of Amati et al. (2002).

Table 1 $E_{iso} - E_{p,i}$ correlation

	This work			Amati
	high	average	low	et al (2002)
K	126	141	159	95
m	0.35	0.45	0.55	0.5

4.2.2 The $L_{iso} - E_{p,i}$ Relation

The relation between the energy $E_{p,i}$ and the isotropic luminosity at peak time, with well-determined redshifts, was found by Yonetoku et al. (2004). It was expressed as:

$$\frac{L_{iso}}{10^{52} \text{ erg/s}} = A \left[\frac{E_{p,i}}{keV} \right]^p. \quad (20)$$

In Figure(7) we plot $E_{p,i}$ vs. L_{iso} in log-log scale for 27 *Swift* bursts with well determined redshifts. We have drawn two extreme straight lines which represent "brackets". From these two lines we deduced the mean values for the slope and the intercept (a and b). In Table (2) we give the constants A and p of Eq.20, which are obtained from the following relations:

$$A = 10^{-\frac{b}{a}+52}, \quad (21)$$

$$p = a^{-1}. \quad (22)$$

For comparison, we also show the original results of Yonetoku et al. (2004).

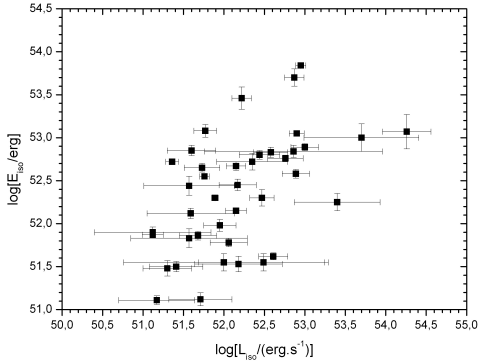


Fig. 5 Plot of $\log E_{iso}$ vs. $\log L_{iso}$: 42 Swift LGRBs have been used in this plot (Tab.3). Here, we did not consider the constraint: $P_{ph} \geq 2.6 \text{ ph/cm}^2/\text{s}$. The error bars over L_{iso} are much larger than those over E_{iso} because of the size of the error bars over the peak flux.

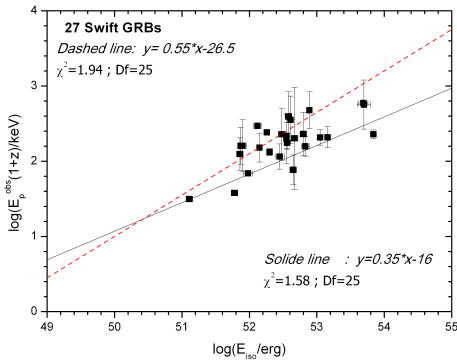


Fig. 6 The $E_{iso} - E_{p,i}$ correlation using 27 Swift LGRBs that satisfy all the constraints that we set.

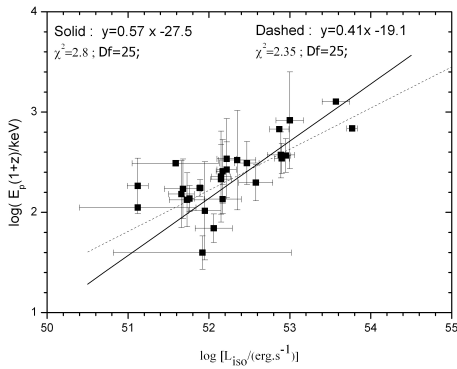


Fig. 7 The $L_{iso} - E_{p,i}$ correlation using 27 Swift LGRBs that satisfy all the constraints that we set

Table 2 $L_{iso} - E_{p,i}$ correlation.

	This work		Yonetoku
	high	average	et al (2004)
$A \times 10^{-5}$	0.38	3.6	4.29 ± 0.15
p	2.44	2.04	1.94 ± 0.19

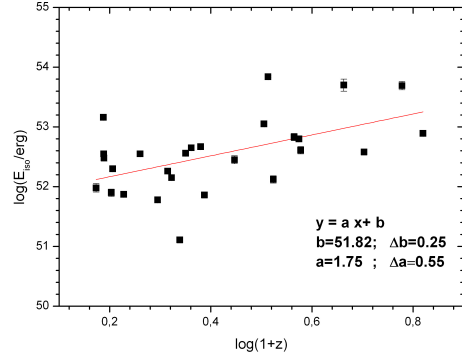


Fig. 8 Evolution of E_{iso} with the redshift z using 27 Swift LGRBs that satisfy all the constraints that we set.

4.2.3 Evolution of L_{iso} and E_{iso} with Redshift

In the sample of 27 Swift LGRBs, we find an interesting evolution of the isotropic energy E_{iso} in terms of the redshift z . We plot the data in Figure (8), showing a trend between E_{iso} and z , a trend which can be expressed by the following equation:

$$\frac{E_{iso}}{\text{erg}} = 10^{51.82 \pm 0.25} (1+z)^{1.75 \pm 0.55}. \quad (23)$$

This result is in good agreement with the recently published paper (Salvaterra et al. 2013). We also find a similar trend between L_{iso} and z , (Figure 9), a trend which can be expressed by the following equation:

$$\frac{L_{iso}}{\text{erg/s}} = 10^{51.2 \pm 0.2} (1+z)^{2.6 \pm 0.5}. \quad (24)$$

It is indeed logical to find a $(1+z)$ dependence in the ratio of L_{iso} and E_{iso} due to the cosmological effect on the duration $T_{90}^{obs} = T_{90}^s (1+z)$, which affects only the luminosity.

5 Discussion

In this section we present a brief review of recent studies that have dealt with the Amati and Yonetoku relations in order to put our study into proper perspective. Some studies (Zhang et al. 2012; Tsutsui et al. 2013)

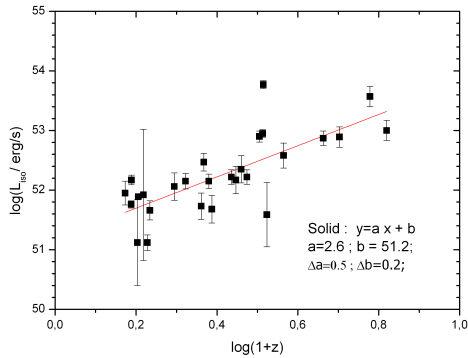


Fig. 9 Evolution of L_{iso} with the redshift z using 27 *Swift* LGRBs that satisfy all the constraints that we set.

have lately considered whether these correlations apply to both short and long bursts. It had previously been thought that the Amati relation applies only to LGRBs, whereas the Yonetoku relation applies to both. In the study by (Zhang and Mészáros 2004) the authors used a sample of 148 LGRBs and 17 SGRBs to investigate this issue for the Yonetoku relation. The results obtained indicate that both the LGRB and SGRB groups seem to adhere to the correlation with the same best-fit: $L_{iso} \propto E_{p,i}^{1.7}$. This implies that the radiation mechanism is similar for short and long bursts, and probably has a quasi-thermal origin in which most of the energy is dissipated close to the central engine. On the other hand, the study by Tsutsui et al. (2013) considered both the Amati and Yonetoku relations but for short bursts only. The authors first clarified the sometimes ambiguous issue of when a burst is to be considered short. They then distinguished between "secure" and "misguided" SGRBs. Out of an initial sample of 13 bursts, 8 were found to be "secure". With these 8 bursts they were able to obtain good fits and to show that both the Amati and Yonetoku relations apply; however, for a given $E_{p,i}$, E_{iso} is dimmer by a factor of about 100, and L_{iso} is dimmer by a factor of about 5 than that known for LGRBs.

Other studies have looked at the possible redshift evolution of these correlations. The study by Geng and Huang (2013) used a sample of 65 bursts to investigate the possible redshift dependence of the low-energy index, α , in the Band function. Their results indicate that such a dependence does exist. Although we did not utilize the Band function in our study, since we used a CPL, our results for the redshift dependence of E_{iso} and L_{iso} are in qualitative agreement with what was found by Geng and Huang (2013).

The study by Nava et al. (2012) used a sample of 47 GRBs to investigate the robustness of the Amati and

Yonetoku relations, and also to look into their possible redshift evolution. Although the authors found some outliers, their conclusion was that these relations are genuine and are not due to selection effects. However, they also found no evolution of these correlations with redshift. This final result is in agreement with a recent study (Azzam and Alotzman 2013) in which the authors investigate the possible redshift evolution of a sample of 65 bursts by binning the data and carrying out the proper z -correction and k -correction. The authors obtained good fits for the binned data, but found no evidence for redshift evolution.

Our current study is in agreement with the above investigations in that it confirms the existence of the Amati and Yonetoku correlations. However, we have taken a step further by demonstrating that applying a stricter criterion for choosing the GRB sample in the first place, actually improves the quality of these fits, since it reduces the dispersion that is commonly seen in these correlations. Therefore, the proper selection of the data sample is crucial in such studies.

6 Conclusion

We have conducted a statistical study of a sample of *Swift* bursts. Among the 229 LGRBs with well-determined redshifts, we selected the 71 GRBs whose observed energy E_p^{obs} is within the energy interval 15-150 keV. Among those, 57 GRBs had L_{iso} and $E_{p,i}$ values and could thus be used to test the Yonetoku relation, while 56 GRBs had E_{iso} and $E_{p,i}$ values and could thus be used for the study of the Amati relation. These bursts satisfy constraints on the energy E_p^{obs} . The uncertainties (error bars) on the bursts' physical quantities were estimated using a Monte Carlo method. We present the data for the bursts, along with the error bars, in a summary table (3). For these bursts, we plotted E_{iso} against $E_{p,i}$ and L_{iso} against $E_{p,i}$, testing the Amati and Yonetoku relations on that sample. We found the data to be tainted with significant dispersions around the linear trends. But by adding a condition on the peak flux, we obtained a sample of 27 LGRBs for which we got good linearities on those two relations.

Acknowledgements

The authors gratefully acknowledge the use of the online *Swift/BAT* table compiled by Taka Sakamoto and Scott D. Barthelmy. We thank the referee for constructive comments, which led us to clarify some aspects of the paper.

References

- Amati, L.: *Mon. Not. R. Astron. Soc.* **372**, 233 (2006). doi:10.1111/j.1365-2966.2006.10840.x
- Amati, L., Frontera, F., Guidorzi, C.: *Astron. Astrophys.* **508**, 173 (2009). 0907.0384. doi:10.1051/0004-6361/200912788
- Amati, L., Frontera, F., Tavani, M., in't Zand, J.J.M., Antonelli, A., Costa, E., Feroci, M., Guidorzi, C., Heise, J., Masetti, N., Montanari, E., Nicastro, L., Palazzi, E., Pian, E., Piro, L., Soffitta, P.: *Astron. Astrophys.* **390**, 81 (2002). doi:10.1051/0004-6361:20020722
- Amati, L., Guidorzi, C., Frontera, F., Della Valle, M., Finelli, F., Landi, R., Montanari, E.: *Mon. Not. R. Astron. Soc.* **391**, 577 (2008). 0805.0377. doi:10.1111/j.1365-2966.2008.13943.x
- Azzam, W.J., Alothman, M.J.: *Advances in Space Research* **38**, 1303 (2006a). doi:10.1016/j.asr.2004.12.019
- Azzam, W.J., Alothman, M.J.: *Nuovo Cimento B Serie* **121**, 1431 (2006b). doi:10.1393/ncb/i2007-10270-5
- Azzam, W.J., Alothman, M.J.: *International Journal of Astronomy and Astrophysics* **3**, 372 (2013). 1303.6530. doi:10.4236/ijaa.2012.21001
- Band, D., Matteson, J., Ford, L., Schaefer, B., Teegarden, B., Cline, T., Paciesas, W., Pendleton, G., Fishman, G., Meegan, C.: In: Paciesas, W.S., Fishman, G.J. (eds.) *American Institute of Physics Conference Series*. American Institute of Physics Conference Series, vol. 265, p. 169 (1992)
- Bloom, J.S., Frail, D.A., Sari, R.: *Astron. J.* **121**, 2879 (2001). astro-ph/0102371. doi:10.1086/321093
- Capozziello, S., Izzo, L.: *Astron. Astrophys.* **490**, 31 (2008). 0806.1120. doi:10.1051/0004-6361:200810337
- Demianski, M., Piedipalumbo, E.: *Mon. Not. R. Astron. Soc.* **415**, 3580 (2011). 1104.5614. doi:10.1111/j.1365-2966.2011.18975.x
- Elliott, J., Greiner, J., Khochfar, S., Schady, P., Johnson, J.L., Rau, A.: *Astron. Astrophys.* **539**, 113 (2012). 1202.1225. doi:10.1051/0004-6361/201118561
- Fenimore, E.E., Ramirez-Ruiz, E.: *ArXiv Astrophysics e-prints* (2000). astro-ph/0004176
- Geng, J.J., Huang, Y.F.: *Astrophys. J.* **764**, 75 (2013). 1212.4340. doi:10.1088/0004-637X/764/1/75
- Ghirlanda, G., Ghisellini, G., Lazzati, D.: *Astrophys. J.* **616**, 331 (2004). doi:10.1086/424913
- Ghirlanda, G., Nava, L., Ghisellini, G.: *Astron. Astrophys.* **511**, 43 (2010). 0908.2807. doi:10.1051/0004-6361/200913134
- Ghirlanda, G., Ghisellini, G., Firmani, C., Celotti, A., Bosnjak, Z.: *Mon. Not. R. Astron. Soc.* **360**, 45 (2005). doi:10.1111/j.1745-3933.2005.00043.x
- Ghirlanda, G., Ghisellini, G., Firmani, C., Nava, L., Tavetchio, F., Lazzati, D.: *Astron. Astrophys.* **452**, 839 (2006). astro-ph/0511559. doi:10.1051/0004-6361:20054544
- Komatsu, E., Dunkley, J., Nolta, M.R., Bennett, C.L., Gold, B., Hinshaw, G., Jarosik, N., Larson, D., Limon, M., Page, L., Spergel, D.N., Halpern, M., Hill, R.S., Kogut, A., Meyer, S.S., Tucker, G.S., Weiland, J.L., Wollack, E., Wright, E.L.: *Astrophys. J. Suppl. Ser.* **180**, 330 (2009). 0803.0547. doi:10.1088/0067-0049/180/2/330
- Liang, E., Zhang, B.: *Astrophys. J.* **633**, 611 (2005). astro-ph/0504404. doi:10.1086/491594
- Nava, L., Salvaterra, R., Ghirlanda, G., Ghisellini, G., Campana, S., Covino, S., Cusumano, G., D'Avanzo, P., D'Elia, V., Fugazza, D., Melandri, A., Sbarufatti, B., Vergani, S.D., Tagliaferri, G.: *Mon. Not. R. Astron. Soc.* **421**, 1256 (2012). 1112.4470. doi:10.1111/j.1365-2966.2011.20394.x
- Norris, J.P., Marani, G.F., Bonnell, J.T.: *Astrophys. J.* **534**, 248 (2000). astro-ph/9903233. doi:10.1086/308725
- Preece, R.D., Briggs, M.S., Mallozzi, R.S., Pendleton, G.N., Paciesas, W.S., Band, D.L.: *Astrophys. J. Suppl. Ser.* **126**, 19 (2000). astro-ph/9908119. doi:10.1086/313289
- Rossi, F., Guidorzi, C., Amati, L., Frontera, F., Romano, P., Campana, S., Chincarini, G., Montanari, E., Moretti, A., Tagliaferri, G.: *Mon. Not. R. Astron. Soc.* **388**, 1284 (2008). 0802.0471. doi:10.1111/j.1365-2966.2008.13476.x
- Salvaterra, R., Campana, S., Covino, S., D'Avanzo, P., Ghirlanda, G., Ghisellini, G., Melandi, A., Tagliaferri, G., Nava, L., Vergani, S.: *ArXiv e-prints* (2013). 1309.2298
- Tsutsui, R., Yonetoku, D., Nakamura, T., Takahashi, K., Morihara, Y.: *Mon. Not. R. Astron. Soc.* **431**, 1398 (2013). 1208.0429. doi:10.1093/mnras/stt262
- Yonetoku, D., Murakami, T., Nakamura, T., Yamazaki, R., Inoue, A.K., Ioka, K.: *Astrophys. J.* **609**, 935 (2004). arXiv:astro-ph/0309217. doi:10.1086/421285
- Zhang, B., Mészáros, P.: *International Journal of Modern Physics A* **19**, 2385 (2004). arXiv:astro-ph/0311321. doi:10.1142/S0217751X0401746X
- Zhang, Z.B., Chen, D.Y., Huang, Y.F.: *Astrophys. J.* **755**, 55 (2012). 1205.2411. doi:10.1088/0004-637X/755/1/55

Table 3 : Flux F_γ isotropic energy E_{iso} and luminosity L_{iso} calculated from the *Swift* data for a sample of 71 GRBs that satisfy our constraints, except for the threshold on the photon flux.

GRB	z	$\text{Log}(\frac{F_\gamma}{\text{erg/cm}^2/\text{s}})$	$\text{Log}(\frac{L_{iso}}{\text{erg/s}})$	$\text{Log}(\frac{E_{iso}}{\text{erg}})$
130610A	2.092	-6.85 ± 0.08	52.40 ± 0.20	
130514A	3.6	-6.67 ± 0.05	52.87 ± 0.12	53.70 ± 0.10
130427B	2.78			52.61 ± 0.06
130420A	1.297	-6.39 ± 0.03	51.73 ± 0.22	52.65 ± 0.05
130215A	0.597	-6.73 ± 0.01	51.12 ± 0.72	51.90 ± 0.06
121128A	2.2	-5.97 ± 0.02	52.90 ± 0.09	53.05 ± 0.03
120815A	2.358	-6.87 ± 0.04	51.57 ± 0.72	51.83 ± 0.11
120811C	2.671	-6.58 ± 0.02	52.58 ± 0.21	52.83 ± 0.06
120724A	1.48	-7.56 ± 0.10	52.49 ± 0.8	51.55 ± 0.10
120712A	4.15	-6.69 ± 0.06	53.13 ± 0.58	
120422A	0.28	-7.26 ± 0.14	49.38 ± 1.20	49.79 ± 0.08
120404A	2.876	-7.12 ± 0.05	52.18 ± 0.08	
120326A	1.798	-6.55 ± 0.017	52.17 ± 0.23	52.45 ± 0.07
120118B	2.943	-6.86 ± 0.037	52.35 ± 0.44	52.72 ± 0.10
111229A	1.381	-7.15 ± 0.08	51.30 ± 0.30	51.48 ± 0.09
111228A	0.7141	-6.1 ± 0.02	51.66 ± 0.16	
111107A	2.893			53.48 ± 0.67
111008A	5			53.69 ± 0.07
110808A	1.348	-7.53 ± 0.12	51.41 ± 0.33	51.50 ± 0.06
110801A	1.858	-7.16 ± 0.05	51.60 ± 0.30	52.85 ± 0.06
110715A	0.82			52.55 ± 0.02
110503A	1.613	-6.91 ± 0.03	51.77 ± 0.14	53.08 ± 0.07
110205A	1.98	-6.57 ± 0.03	52.22 ± 0.12	
110128A	2.339	-7.17 ± 0.1	51.59 ± 0.54	52.12 ± 0.06
100906A	1.727	-6.57 ± 0.07	52.22 ± 0.12	
100621A	0.542	-6.02 ± 0.01	51.76 ± 0.06	52.55 ± 0.03
100615A	1.398	-6.41 ± 0.03	52.15 ± 0.12	52.67 ± 0.05
100513A	4.772			53.00 ± 0.03
100425A	1.755	-7.17 ± 0.05	52.00 ± 1.24	51.55 ± 0.10
100418A	0.624			50.83 ± 0.05
100316B	1.18	-7.12 ± 0.04	51.17 ± 0.47	51.11 ± 0.05
091208B	1.063			52.26 ± 0.04
091127	0.49	-5.51 ± 0.03	51.95 ± 0.20	51.98 ± 0.07
091029	2.752	-6.94 ± 0.03	52.44 ± 0.25	52.80 ± 0.05
091018	0.971	-6.23 ± 0.17	52.06 ± 0.23	51.78 ± 0.05
090927	1.37	-6.88 ± 0.06	51.71 ± 0.40	51.12 ± 0.08
090926B	1.24			52.56 ± 0.02
090726	2.71	-7.41 ± 0.20	53.40 ± 0.53	52.25 ± 0.10
090618	0.54			53.16 ± 0.02
090424	0.544			52.48 ± 0.05
090423	8.0	-6.93 ± 0.04	52.76 ± 0.22	52.76 ± 0.04
081221	2.26	-5.83 ± 0.02	52.95 ± 0.06	53.84 ± 0.02
081121	2.512	-6.49 ± 0.16	54.26 ± 0.30	
081118	2.58	-7.40 ± 0.10	51.57 ± 0.56	
080916A	0.689	-6.61 ± 0.04	51.12 ± 0.13	51.87 ± 0.03
080520	1.545	-7.60 ± 0.12	51.27 ± 1.43	
080413B	1.1	-5.85 ± 0.03	52.15 ± 0.13	52.15 ± 0.03
80330	1.51			51.64 ± 0.06
080310	2.427	-7.11 ± 0.14	52.49 ± 0.70	
071122	1.14	-7.64 ± 0.18	50.33 ± 0.44	51.46 ± 0.08
071117	1.331	-5.99 ± 0.02	52.47 ± 0.15	
071010A	0.98	-7.47 ± 0.13	49.90 ± 0.59	50.70 ± 0.05
070611	2.04	-7.30 ± 0.08	52.61 ± 0.18	51.62 ± 0.04
070506	2.31	-7.23 ± 0.12	52.18 ± 0.54	
070419A	0.97	-8.04 ± 0.18	49.51 ± 0.55	51.21 ± 0.04
070129	2.338	-7.48 ± 0.06	51.36 ± 0.08	52.72 ± 0.03
061222B	3.355	-7.08 ± 0.11	52.86 ± 1.10	52.84 ± 0.07
060927	5.6	-6.62 ± 0.04	53.00 ± 0.17	52.89 ± 0.04
060926	3.208	-7.26 ± 0.11	52.64 ± 0.70	
060908	1.884	-6.56 ± 0.05	52.35 ± 0.23	
060604	2.136			51.82 ± 0.07
060526	3.21	-6.88 ± 0.08	53.70 ± 0.71	53.00 ± 0.16
060512	0.443	-7.42 ± 0.09	50.44 ± 1.50	50.10 ± 0.14
060510B	4.9			53.48 ± 0.04
060218	0.033	-7.90 ± 0.14	46.53 ± 1.42	48.52 ± 0.08
060206	4.045	-6.70 ± 0.03	52.89 ± 0.17	52.58 ± 0.05
060115	3.53			52.75 ± 0.06
050525A	0.606	-5.46 ± 0.12	51.89 ± 0.04	52.30 ± 0.01
050416A	0.653	-6.65 ± 0.10	51.92 ± 1.10	
050406	2.44	-7.77 ± 0.12	50.93 ± 1.60	50.90 ± 0.09
050318	1.44	-6.66 ± 0.03	51.68 ± 0.23	51.86 ± 0.05

Table 4 : Data for 71 *Swift* GRBs.

GRB	z	T_{90} sec	Fluence* 10^{-7} erg/cm ²	1s - flux ph/cm ² /s	α 1s Pic spec	E_p^{obs} keV 1s Pic Spec	α_m Aver.Spec	E_{pm}^{obs} keV Aver.Spec
130610A	2.092	46.4	25 ± 1	1.7 ± 0.2	0.202 ± 0.798	93.7 ± 65.3	1.026 ± 0.284	217.1 ± 62.8
130514A	3.6	204	91 ± 2	2.8 ± 0.3	1.173 ± 0.506	146.9 ± 1.0	1.646 ± 0.193	122.9 ± 40.2
130427B	2.78	27	15 ± 1	3 ± 0.4	1.182 ± 0.646	176.3 ± 1.0	1.229 ± 0.594	93.8 ± 29.6
130420A	1.297	123.5	71 ± 3	3.4 ± 0.2	1.030 ± 0.486	58.0 ± 15.6	1.518 ± 0.251	33.4 ± 6.6
130215A	0.597	65.7	54 ± 5	2.5 ± 0.7	0.162 ± 2.978	69.9 ± 1.0	1.126 ± 0.545	100.5 ± 34.8
121128A	2.2	23.3	69 ± 4	12.9 ± 0.4	0.494 ± 0.225	107.7 ± 16.2	1.320 ± 0.183	64.6 ± 6.8
120815A	2.358	9.7	4.9 ± 0.7	2.2 ± 0.3	1.222 ± 1.091	45.7 ± 1.0	1.033 ± 1.259	28.6 ± 1.0
120811C	2.671	26.8	30 ± 3	4.1 ± 0.2	1.015 ± 0.458	53.9 ± 9.8	1.401 ± 0.303	42.9 ± 5.7
120724A	1.48	72.8	6.8 ± 1.1	0.6 ± 0.2	-2.910 ± 0.100	41.1 ± 10.0	0.534 ± 1.529	27.6 ± 7.5
120712A	4.15	14.7	18 ± 1	2.4 ± 0.2	0.133 ± 0.742	99.7 ± 55.8	0.984 ± 0.306	143.2 ± 158.6
120422A	0.28	5.35	2.3 ± 0.4	0.6 ± 0.2	-0.558 ± 2.948	103.6 ± 34.1	0.398 ± 1.099	91.5 ± 30.7
120404A	2.876	38.7	16 ± 1	1.2 ± 0.2	2.052 ± 0.100	21.5 ± 1.0	1.821 ± 0.100	269.3 ± 1.0
120326A	1.798	69.6	26 ± 3	4.6 ± 0.2	1.127 ± 0.410	48.4 ± 6.9	1.409 ± 0.338	41.1 ± 6.9
120118B	2.943	23.26	18 ± 1	2.2 ± 0.3	1.434 ± 1.085	50.7 ± 1.0	1.599 ± 0.506	39.0 ± 1.0
111229A	1.3805	25.4	3.4 ± 0.7	1 ± 0.2	1.379 ± 1.046	108.1 ± 1.0	1.764 ± 0.904	102.7 ± 1.0
111228A	0.7141	101.2	85 ± 2	12.4 ± 0.5	1.650 ± 0.272	88.7 ± 29.7	1.989 ± 0.100	1.9 ± 7.2
111107A	2.893	26.6	8.8 ± 0.8	1.2 ± 0.2	1.034 ± 0.630	782.8 ± 1.0	2.285 ± 0.198	102.1 ± 1.0
111008A	5	63.46	53 ± 3	6.4 ± 0.7	1.011 ± 0.539	212.3 ± 1.0	1.725 ± 0.338	98.7 ± 1.0
110808A	1.348	48	3.3 ± 0.8	0.4 ± 0.2	0.168 ± 1.113	65.8 ± 1.0	1.854 ± 0.100	11.5 ± 1.0
110801A	1.858	385	47 ± 3	1.1 ± 0.2	1.646 ± 0.939	62.5 ± 1.0	1.615 ± 0.296	78.6 ± 26.2
110715A	0.82	13	118 ± 2	53.9 ± 1.1	0.985 ± 0.131	152.0 ± 32.6	1.254 ± 0.116	119.8 ± 20.8
110503A	1.613	10	100 ± 4	1.35 ± 0.06	0.100 ± 0.356	111.8 ± 21.9	0.881 ± 0.254	133.1 ± 54.5
110205A	1.98	257	170	3.6 ± 0.2	1.219 ± 0.344	144.6 ± -46.0	1.527 ± 0.185	94.2 ± 61.5
110128A	2.339	30.7	7.2 ± 1.4	0.8 ± 0.2	0.052 ± 2.242	92.5 ± 0.0	0.265 ± 2.001	88.4 ± 0.0
100906A	1.727	114.4	120 ± 0.1	10.1 ± 0.4	0.876 ± 0.294	97.9 ± 26.9	1.655 ± 0.149	108.6 ± 109.4
100621A	0.542	63.6	210 ± 0.1	12.8 ± 0.3	0.918 ± 0.143	89.0 ± 11.6	1.814 ± 0.114	128.3 ± 42.2
100615A	1.398	39	50 ± 1	5.4 ± 0.2	1.157 ± 0.245	94.8 ± 43.5	1.647 ± 0.176	84.0 ± 57.4
100513A	4.772	84	14 ± 1	0.6 ± 0.1	1.253 ± 0.100	939.1 ± 1.0	1.364 ± 0.437	115.6 ± 1.0
100425A	1.755	37	4.7 ± 0.9	1.4 ± 0.2	-0.351 ± 2.407	30.2 ± 5.9	0.847 ± 1.670	26.6 ± 1.0
100418A	0.6235	7	3.4 ± 0.5	1 ± 0.2	1.982 ± 0.100	1.1 ± 1.0	1.920 ± 0.100	18.5 ± 1.0
100316B	1.18	3.8	2 ± 0.2	1.3 ± 0.1	1.530 ± 0.730	30.2 ± 21.7	1.858 ± 0.496	14.4 ± 1.0
091208B	1.063	14.9	33 ± 2	15.2 ± 1.0	1.315 ± 0.351	255.5 ± 1.0	1.595 ± 0.338	116.9 ± 1.0
091127	0.49	7.1	90 ± 3	46.5 ± 2.7	1.329 ± 0.399	69.5 ± 34.2	1.797 ± 0.280	46.3 ± 1.0
091029	2.752	39.2	24 ± 1	1.8 ± 0.1	0.923 ± 0.652	52.8 ± 17.7	1.465 ± 0.275	61.3 ± 17.6
091018	0.971	4.4	14 ± 1	10.3 ± 0.4	1.296 ± 0.306	35.2 ± 5.0	1.765 ± 0.242	19.2 ± 1.0
090927	1.37	2.2	2 ± 0.3	2 ± 0.2	0.682 ± 0.977	56.0 ± 36.4	1.303 ± 0.649	61.8 ± 1.0
090926B	1.24	109.7	73 ± 2	3.2 ± 0.3	0.819 ± 0.594	177.2 ± 1.0	0.517 ± 0.236	78.2 ± 7.0
090726	2.71	67	8.6 ± 1	0.7 ± 0.2	-1.928 ± 0.278	40.3 ± 9.0	1.345 ± 0.858	27.3 ± 1.0
090618	0.54	113.2	1050 ± 10	38.9 ± 0.8	1.153 ± 0.144	170.4 ± 68.7	1.414 ± 0.081	134.7 ± 19.1
090424	0.544	48	210 ± 1	71 ± 2	0.915 ± 0.137	166.0 ± 52.6	1.244 ± 0.140	147.8 ± 51.3
090423	8.0	10.3	5.9 ± 0.4	1.7 ± 0.2	1.199 ± 0.515	84.5 ± 28.6	0.765 ± 0.470	53.2 ± 7.0
081221	2.26	34	181 ± 3	18.2 ± 0.5	0.749 ± 0.190	112.9 ± 19.3	1.211 ± 0.128	69.9 ± 3.9
081121	2.512	14	41 ± 3	4.4 ± 1	-2.441 ± 0.100	56.8 ± 8.0	0.563 ± 0.500	140.3 ± 126.8
081118	2.58	67	12 ± 1	0.6 ± 0.2	1.246 ± 1.723	72.3 ± 1.0	1.569 ± 0.619	34.3 ± 24.9
080916A	0.689	60	40 ± 1	2.7 ± 0.2	0.031 ± 0.468	108.7 ± 30.3	1.167 ± 0.206	94.7 ± 23.2
080520	1.545	2.8	0.55 ± 0.17	0.5 ± 0.1	0.418 ± 2.495	28.7 ± 21.0	1.742 ± 1.450	7.1 ± 13.1
080413B	1.1	8	32 ± 1	18.7 ± 0.8	1.005 ± 0.291	102.0 ± 35.5	1.222 ± 0.276	72.2 ± 13.9
080330	1.51	61	3.4 ± 0.8	0.9 ± 0.2	1.984 ± 0.372	1.4 ± 1.0	1.863 ± 0.100	7.5 ± 1.0
080310	2.4266	365	23 ± 2	1.3 ± 0.2	0.669 ± 1.454	41.9 ± 17.5	1.945 ± 0.522	5.5 ± 14.5
071122	1.14	68.7	5.8 ± 1.1	0.4 ± 0.2	1.985 ± 0.100	3.2 ± 1.0	1.423 ± 0.937	79.4 ± 1.0
071117	1.331	6.6	24 ± 1	11.3 ± 0.4	0.339 ± 0.256	133.0 ± 28.4	1.232 ± 0.244	127.2 ± 94.0
071010A	0.98	6	2 ± 0.4	0.8 ± 0.3	1.992 ± 0.100	1.0 ± 1.0	0.687 ± 0.100	35.6 ± 1.0
070611	2.04	12.2	3.91 ± 0.57	0.82 ± 0.21	-1.819 ± 0.100	46.2 ± 8.9	0.374 ± 0.100	57.7 ± 1.0
070506	2.31	4.3	2.1 ± 0.23	0.96 ± 0.13	-0.045 ± 1.227	47.3 ± 12.0	0.924 ± 0.770	57.8 ± 50.6
070419A	0.97	115.6	5.58 ± 0.83	0.2 ± 0.1	1.975 ± 0.100	1.4 ± 1.0	1.101 ± 0.100	24.3 ± 1.0
070129	2.338	460.6	29.8 ± 2.67	0.55 ± 0.12	1.445 ± 0.100	43.5 ± 1.0	1.390 ± 0.100	40.9 ± 1.0
061222B	3.355	40	22.4 ± 1.83	1.59 ± 0.36	0.635 ± 2.486	29.1 ± 21.1	1.296 ± 0.565	46.7 ± 15.7
060927	5.6	22.5	11.3 ± 0.68	2.7 ± 0.17	0.339 ± 0.462	125.4 ± 60.5	0.919 ± 0.378	72.0 ± 17.6
060926	3.208	8	2.19 ± 0.25	1.09 ± 0.14	1.689 ± 1.029	15.5 ± 16.0	1.984 ± 0.100	1.0 ± 10.3
060908	1.884	19.3	28 ± 1.11	3.03 ± 0.25	0.134 ± 0.614	115.2 ± 57.1	0.967 ± 0.269	150.7 ± 112.4
060604	2.1357	95	4.02 ± 1.06	0.34 ± 0.13	1.650 ± 0.100	177.4 ± 1.0	1.533 ± 0.100	34.0 ± 1.0
060526	3.21	298.2	12.6 ± 1.65	1.67 ± 0.18	0.247 ± 0.916	84.8 ± 59.6	2.058 ± 0.100	27.9 ± 1.0
060512	0.4428	8.5	2.32 ± 0.4	0.88 ± 0.2	-0.163 ± 2.503	22.9 ± 11.1	1.011 ± 1.752	23.0 ± 16.0
060510B	4.9	275.2	40.7 ± 1.76	0.57 ± 0.11	1.381 ± 1.419	944.0 ± 1.0	1.494 ± 0.289	96.1 ± 1.0
060218	0.033	2100	15.7 ± 1.52	0.25 ± 0.11	0.201 ± 2.175	29.1 ± 18.5	0.201 ± 2.175	29.1 ± 18.5
060206	4.045	7.6	8.31 ± 0.42	2.79 ± 0.17	0.746 ± 0.427	74.0 ± 17.0	1.165 ± 0.325	78.1 ± 25.6
060115	3.53	139.6	17.1 ± 1.5	0.87 ± 0.12	1.279 ± 1.178	669.6 ± 1.0	1.026 ± 0.524	62.4 ± 23.1
050525A	0.606	8.8	153 ± 2.21	41.7 ± 0.94	0.584 ± 0.144	109.0 ± 9.0	0.981 ± 0.118	82.3 ± 3.7
050416A	0.653	2.5	3.67 ± 0.37	4.88 ± 0.48	-0.513 ± 1.710	24.1 ± 4.1	1.233 ± 1.201	13.0 ± 10.3
050406	2.44	5.4	0.68 ± 0.14	0.36 ± 0.1	0.054 ± 2.505	26.2 ± 18.6	-0.102 ± 2.331	27.9 ± 10.7
050318	1.44	32	10.8 ± 0.77	3.16 ± 0.2	0.882 ± 0.459	70.3 ± 20.9	1.219 ± 0.434	51.3 ± 11.2